Laser trapping in anisotropic fluids and polarization-controlled particle dynamics

Ivan I. Smalyukh*†‡§, Aliaksandr V. Kachynski*, Andrey N. Kuzmin*, and Paras N. Prasad*§

*Institute for Lasers, Photonics, and Biophotonics, University at Buffalo, State University of New York, Buffalo, NY 14260-3000; †Chemical Physics Interdisciplinary Program and Liquid Crystal Institute, Kent State University, Kent, OH 44242; and ‡Department of Materials Science and Engineering, University of Illinois at Urbana–Champaign, Urbana, IL 61801

Anisotropic fluids are widespread, ranging from liquid crystals used in displays to ordered states of a biological cell interior. Optical trapping is potentially a powerful technique in the fundamental studies and applications of anisotropic fluids. We demonstrate that laser beams in these fluids can generate anisotropic optical trapping forces, even for particles larger than the trapping beam wavelength. Immersed colloidal particles modify the fluid's ordered molecular structures and locally distort its optic axis. This distortion produces a refractive index "corona" around the particles that depends on their surface characteristics. The laser beam can trap such particles not only at their center but also at the high-index corona. Trapping forces in the beam's lateral plane mimic the corona and are polarization-controlled. This control allows the optical forces to be reversed and cause the particle to follow a prescribed trajectory. Anisotropic particle dynamics in the trap varies with laser power because of the anisotropy of both viscous drag and trapping forces. Using thermotropic liquid crystals and biological materials, we show that these phenomena are quite general for all anisotropic fluids and impinge broadly on their quantitative studies using laser tweezers. Potential applications include modeling thermodynamic systems with anisotropic polarization-controlled potential wells, producing optically tunable photonic crystals, and fabricating light-controlled nano- and micropumps.

colloids | laser tweezers | liquid crystals | optical trapping | defects

Anisotropic fluids have properties intermediate between those of liquids and solid crystals (1). Flowing like liquids, they are composed of anisotropic molecules and exhibit long range orientational order as well as varying degrees of positional order (1–4). The average molecular orientation is described by a director $\hat{N}$ (1), which is an optic axis in the most common anisotropic fluids, the uniaxial liquid crystals (LCs). LCs are widely known for their applications in displays, telecommunications, and electro-optic devices (1). However, membranes, cytoskeleton proteins, amino acids, viruses, and lipids can form LC phases not only *in vitro* but even *in vivo*, ranging from self-organized structures of collagen in cornea (5) to nematic-like actin and myosin organization in muscle fibers (4), and to ordered structures in human spermatozoa (6, 7). Anisotropic fluids have medical applications in drug delivery (8), and also have relevance to diseases such as atherosclerosis (4) and cystic fibrosis (9). Many materials of our household commodities, such as soaps, detergents, dyes, food products, and colorants, exhibit LC polymorphism when dissolved in water (1, 4). Anisotropic polymer fluids form during DNA droplet drying in "gene chips" (10) as well as in spider silk with unique mechanical properties (11). Anisotropic suspensions (12, 13) and phases of bent-core molecules (14) have attracted a great deal of attention because of their unique properties and potential applications. Anisotropic self-organization in a living cell's interior may play a vital biological function and is readily observed by means of birefringence imaging (15, 16). Recently, there has been a growing interest in optical trapping in anisotropic media (17–22). Laser tweezers can control dynamics of nano- and micro-objects and allow for measurement of colloidal forces (2, 23) mediated by LC elasticity (12, 19). Therefore, fundamental study of laser trapping properties in anisotropic fluids is of great significance.

In this article, we demonstrate that optical trapping of colloidal spheres in anisotropic fluids is direction sensitive and can be controlled by changing polarization of the beam. The unique trapping properties arise because of the following factors. A linearly polarized beam propagating in the anisotropic fluid "sees" the local effective refractive index n_{eff} that depends on the director $\hat{N}$ and the light polarization state. A spherical particle in the LC with a uniform far-field director $\hat{N}_0$ causes local director distortions, which produce a refractive index "corona" (RIC), different from n_{eff} index far from the sphere. By controlling the particle's surface characteristics, we generate well defined structures around the spheres and demonstrate that the angular pattern of trapping forces mimics that of the RIC. Trapping of the beads depends on the director structure, which can be changed by surface treatment of the particles or applying an external field (24). The direction-sensitive trapping resembles that of objects with an anisotropic shape such as discs and rods. Optical forces are varied by changing beam polarization, even up to an extreme situation when a particle is trapped at some polarizations, but repelled from the beam with other polarization states. Control of particle dynamics by polarization of a stationary trap has potential optomechanic and photonic applications.

Results

Director Structure and RIC Around Beads. Fig. 1 shows optical polarizing microscopy (PM) images of particles with different RICs. In each image's pixel (Fig. 1 *A–D*), light intensity $I_{PM} \propto \sin^2(2\beta)\sin^2[(\pi/\lambda)\int_0^h n_{eff}(z)dz - n_o]$ is related to the local index n_{eff} averaged across the chamber thickness h, where β is the angle between the local director and a polarizer in PM. Experimental images are consistent with director structures (Fig. 1 *E–L*) that we computer-simulate by using the *Ansatzen* minimizing the Frank elastic free energy (12, 13, 25, 26) for respective boundary conditions at the particle's surface. We also calculate the patterns of n_{eff} for laser light linearly polarized perpendicular to the far-field director $\hat{N}_0$ (Fig. 1 *E–H*) and parallel to it (Fig. 1 *I–L*). Clearly, the RICs around beads are polarization dependent (Fig. 1 *E–L*).

Surface treatment and confinement allow us to control the director $\hat{N}$ and RIC (Fig. 1). The particles with tangential boundary conditions (Fig. 1*A*) produce a quadrupolar pattern of $\hat{N}$ and RIC (19). At the bead–LC interface, $\hat{N}$ is parallel to the surface and continuously transforms to the far-field director $\hat{N} \parallel \hat{N}_0$ far from the

© 2006 by The National Academy of Sciences of the USA
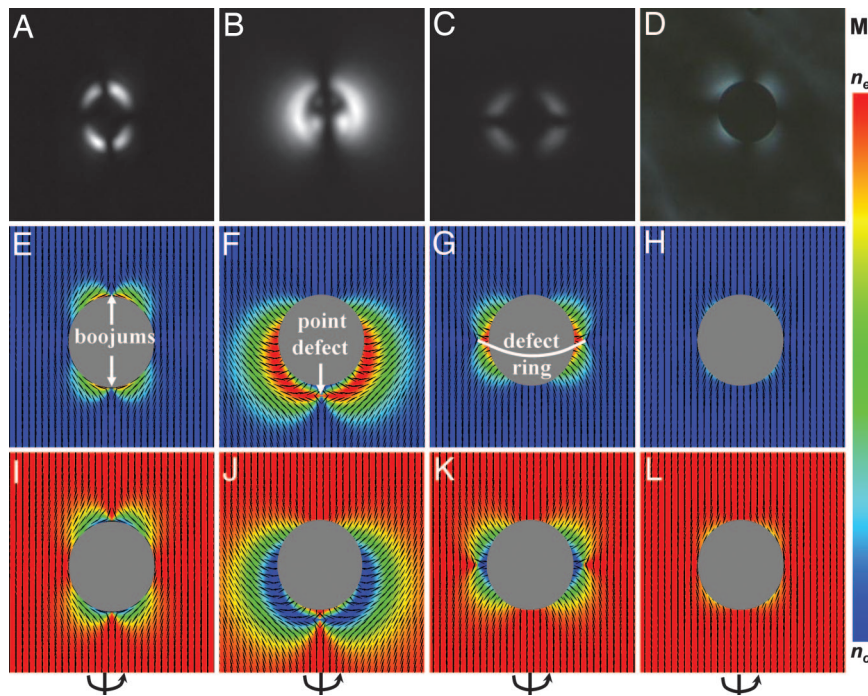
www.pnas.org/cgi/doi/10.1073/pnas.0608698103

Fig. 1. Particles in anisotropic fluids. (*A–D*) PM images of the director around beads with $R = 1.5$ μm and strong tangential surface anchoring in 4-*n*-pentyl-4′-cyanobiphenyl (5CB) (*A*), $R = 1$ μm and strong perpendicular anchoring when confined into the $h = 30$ μm chamber with AMLC-0010 (an LC material from AlphaMicron, Kent, OH) (*B*), $R = 1$ μm and perpendicular anchoring in the $h = 6$ μm chamber with AMLC-0010 (*C*), and with weak tangential anchoring in an anisotropic λ-DNA solution (*D*). (*E–L*) Computer-simulated director $\hat{N}$ structures corresponding to *A–D* and respective RICs for polarizations $\hat{P} \perp \hat{N}_0$ (*E–H*) and $\hat{P} \parallel \hat{N}_0$ (*I–L*). (*M*) Color scale of index n_{eff} varying from n_o to n_e. Ellipsoids in *E–L* show molecular orientations and $\hat{N}$; crossed polarizer and analyzer are along image edges in *A–D*. Defects are marked in *E–G* and the symmetry axes are shown in *I–L*.

bead (Fig. 1 *E* and *I*). The only defects are two surface point defects (called "boojums") at the poles of a particle along $\hat{N}_0$. The colloidal beads that align $\hat{N}$ perpendicular to their surfaces can produce dipolar (Fig. 1*B*) or quadrupolar (Fig. 1*C*) director structures and RICs; the structure type is controlled by the particle confinement into chambers of different thickness h (13). A dipole-type structure is formed in thick chambers of $h = 30$ μm much larger than the particle radius $R = 1$ μm (Fig. 1*B*); the bead is accompanied by a point defect in $\hat{N}$, the hyperbolic hedgehog. A quadrupolar "Saturn-ring" configuration is observed in an h = 6 μm cell and contains a line defect (the disclination of a half-integer strength) encircling the particle in the equatorial plane perpendicular to $\hat{N}_0$ (Fig. 1 *C*, *G*, and *K*). Finally, when surface anchoring forces are weak compared with bulk elastic forces, the uniform director structure is barely perturbed by the beads and $\hat{N}$ strongly deviates from the tangential (Fig. 1 *D* and *L*) or perpendicular (Fig. 1*H*) orientations at their surfaces.

All director structures in Fig. 1 have a rotational symmetry axis crossing the particle's center parallel to the far-field director $\hat{N}_0$. The respective RICs have a mirror symmetry plane orthogonal to the substrates and crossing the particle's center parallel to $\hat{N}_0$. In the case of dipolar beads (Fig. 1 *B*, *F*, and *J*) the director distortions slowly decay with distance r from the particle's center and $\hat{N}$ is uniform only at $r \gg R$. Quadrupolar colloids with strong surface anchoring (Fig. 1 *A*, *E*, and *I* and *C*, *G*, and *K*) distort $\hat{N}$ up to $r \sim 3R$; quadrupolar beads with weak anchoring only slightly perturb $\hat{N}$ at $r < 2R$ (Fig. 1 *D*, *H*, and *L*). The RIC size is also the largest for dipolar beads (Fig. 1 *F* and *J*) and is the smallest for the quadrupoles with weak anchoring (Fig. 1 *H* and *L*). The structures shown in Fig. 1 can form in different materials, regardless of whether the material is an aqueous DNA solution or a thermotropic LC. The index n_{eff} depends on light polarization (compare the index patterns in Fig. 1 *E–H* and Fig. 1 *I–L*), which leads to unique optical trapping properties.

Polarization-Controlled Particle Motion. Particles with an index between the ordinary and extraordinary LC indices ($n_o < n_p < n_e$) are either attracted to a stationary laser trap or repelled from it, depending on the beam's polarization $\hat{P}$ (Fig. 2). This behavior is observed, for example, for glass beads with index $n_p \approx 1.51$, which is between n_o and n_e of AMLC-0010 (Table 1). By switching polarization between $\hat{P} \perp \hat{N}_0$ (bead is attracted until trapped) and $\hat{P} \parallel \hat{N}_0$ (bead is repelled), one controls particle motion into or away from the focused beam (Fig. 2 *A* and *D*); the repulsion/attraction cycles can be repeated many times. Dipolar colloids "feel" the beam at distances $r \gg R = 1$ μm (Fig. 2 *A* and *C*); by varying the time interval between the polarization switching, one can control the particle-beam separation up to ≈ 6 μm (Fig. 2*A*). In contrast, quadrupolar colloids feel attractive/repulsive forces at distances only slightly larger than $R = 1$ μm (Fig. 2*D*). This behavior is consistent with the respective RIC sizes of the colloids (Fig. 1) discussed above.

Trajectories of particle motion depend on the gradients of the index n_{eff} in the RICs, which change upon switching polarization between $\hat{P} \perp \hat{N}_0$ and $\hat{P} \parallel \hat{N}_0$. Therefore, the attraction and repulsion trajectories are usually different, reflecting dipolar (Fig. 2*C*) or quadrupolar (Fig. 2*E*) RIC symmetries at respective polarizations. A slight variation of the trajectories from cycle to cycle is due to the Brownian motion when the bead is far from the trap. With essentially the same probability, the particle can follow trajectories

Table 1. Materials and their refractive indices

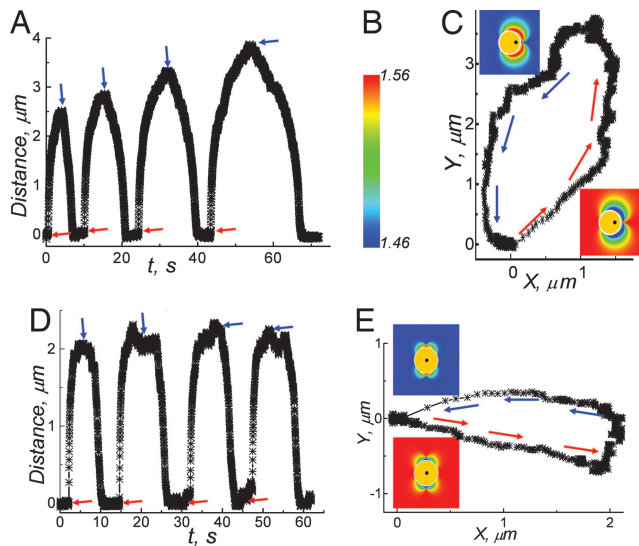| Material	Refractive index			Source
	n_o	n_e	$\bar{n}_{\text{LC}}$	
5CB	1.54	1.74	1.61	EM Chemicals
AMLC-0010	1.47	1.55	1.50	AlphaMicron

Smalyukh *et al.*

PHYSICS

Fig. 2. Polarization-controlled particle motion into or away from the stationary laser trap. (*A*) Distance to the trap vs. time. (*B*) Color scale of index n_{eff}. (*C*) Motion trajectory of a dipolar bead as polarization is switched between orthogonal directions. (*D*) Distance to the trap center vs. time. (*E*) Motion trajectory of a quadrupolar bead. Red and blue arrows in *A* and *D* indicate times of switching polarization to $\hat{P} \parallel \hat{N}_0$ and $\hat{P} \perp \hat{N}_0$, respectively; arrows in *C* and *E* show motion directions corresponding to one of the repulsion/attraction cycles in *A* and *D* at respective polarizations. $\hat{N}_0$ is along the *x* axis.

that would be mirror images of those shown in Fig. 2 *C* and *E* with respect to the RIC's mirror symmetry plane (*x* axis in Fig. 2 *C* and *E*). This demonstrates that because of the well controlled RIC around beads, a focused beam can set a particle to "swim" and follow a prescribed polarization-controlled trajectory.

Multistability of Optical Trapping. Unlike a particle in an isotropic medium, a particle in an anisotropic fluid is not necessarily trapped at its center. To probe this phenomenon, we studied particle positions with respect to the initial trapping point (Fig. 3A) when the laser beam is suddenly shifted between locations such as those marked by white filled circles in Fig. 3 *B–D*. Depending on the direction of approaching the trap, the bead can be trapped at a point slightly shifted from its center along the director symmetry axis (Fig. 3 *A* and *B*) or at one of the RIC wings with high index n_{eff} (Fig. 3 *A*, *C*, and *D*) (apparently, outside of the actual bead). For shifts at
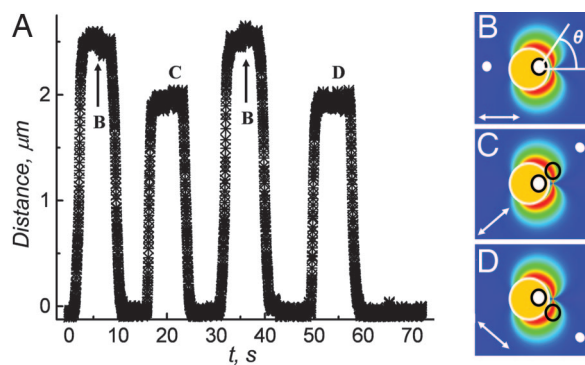

Fig. 3. Trapping of dipolar colloids at the bead or RIC. (*A*) Distance from the initial trapping point (colocalized white filled and black open circles in *B–D*) vs. time as the beam is suddenly shifted to locations shown by white filled circles and back. The bead's trapping point (open black circle) in *B–D* is different, depending on the direction from which a bead approaches the trap. The color scale of n_{eff} is the same as in Fig. 2; $\hat{N}_0$ is horizontal in *B–D*.
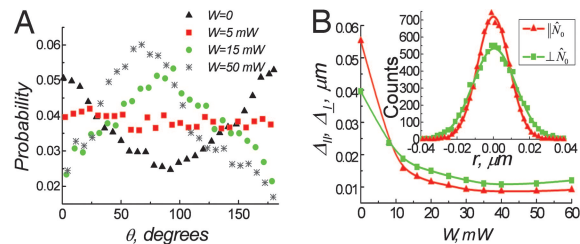

Fig. 4. Particle dynamics. (*A*) Probability of particle displacement vs. angle θ for a glass bead in AMLC-0010 at various laser power inputs, *W*. (*B*) Distribution widths $\Delta_\parallel$, $\Delta_\perp$ of particle displacements in directions parallel/perpendicular to $\hat{N}_0$. (*Inset*) Displacement histograms for *W* = 30 mW.

angles $\theta = \pm(10\text{–}110)°$ to $\hat{N}_0$, the trapping point (marked by an open black circle) is at one of the high-index RIC wings in Fig. 3 *C* and *D* rather than within the bead (Fig. 3*B*) observed otherwise. Optical trapping at all three points is stable over time because the high-index RIC wings are separated from the bead and each other by regions of low index n_{eff} (Fig. 3 *B–D*). One therefore can expect local/global minima in the trapping potential corresponding to the three trapping points. By varying indices n_p, n_e, and n_o and/or by changing polarization, one can control stability of different trapping sites. For example, when a glass particle is immersed in 5CB with $n_e > n_o > n_p$, unexpectedly, the trapping is still possible for polarization orthogonal to $\hat{N}_0$, but there are only two stable trapping points at the high-index RIC wings. In contrast, when a melamine resin (MR) bead is trapped in AMLC-0010 with $n_p > n_e > n_o$, the only stable trapping point is within the particle, slightly shifted from its center to the hyperbolic point defect (Fig. 3*B*).

Colloids with different director structures also exhibit trapping properties that strongly depend on the RIC. For example, quadrupolar colloids in Fig. 1 *A*, *C*, and *D* can have one stable trapping point at the particle center, or two stable points at the two opposite RIC wings with high index n_{eff}, or even four trapping points at the four high-index wings, depending on director structure and refractive indices involved. Moreover, the location and relative stability of the trapping points are polarization controlled and will be described elsewhere.

Trap Stiffness and Particle Dynamics. To get an insight into the trap stiffness properties, we have studied Brownian motion of a dipolar colloid with index $n_o < n_p < n_e$. We analyze microscopic images and determine both distance and the angle θ to $\hat{N}_0$ of the particle's displacements during time intervals $\tau = 10$ ms over 5–10 min. Using data from 7,000–20,000 images, we obtain the displacement probabilities for different θ (Fig. 4*A*) and construct displacement histograms for directions along and perpendicular to $\hat{N}_0$ (*Inset* of Fig. 4*B*). The distribution widths $\Delta_\parallel$ and $\Delta_\perp$ in Fig. 4*B* are obtained from a Gaussian fitting of these histograms. The dynamics of a microsphere trapped in LC is strongly anisotropic and strikingly different from that in isotropic fluids, where the displacements are direction insensitive and homogeneously decrease with increasing power (2). The anisotropy of particle dynamics in LCs is influenced by both viscous drag and trapping forces, and it is reversed as power increases within $W = 0\text{–}60$ mW (Fig. 4).

The stochastic random force F_{SR} experienced by a bead because of thermal molecular motions is balanced by the viscous drag and the trapping force, $F_{SR} = F_{VD} + F_t(W)$, where we neglect the inertia effects. For directions along and perpendicular to $\hat{N}_0$, $F_{VD\parallel/\perp} = \gamma_{\parallel/\perp}\, \partial r/\partial t$ and $F_{t\parallel/\perp}(W) = \alpha_{\parallel/\perp}(W)r$, where $\gamma_{\parallel/\perp} = 6\pi\eta_{\parallel/\perp}R = k_B T/D_{\parallel/\perp}$ is the drag coefficient, $\eta_{\parallel/\perp}$ is an effective viscosity, k_B is the Boltzmann constant, and T is the thermodynamic temperature; we assume a harmonic trap potential with stiffness $\alpha_{\parallel/\perp}$. When $W = 0$, the diffusion of a dipolar colloid is easier and the displacement probability is larger along
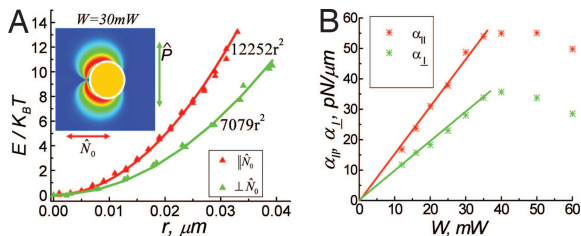
Smalyukh *et al.*

Fig. 5. Anisotropic trap stiffness. (*A*) Trapping potential for directions parallel/perpendicular to $\hat{N}_0$. *Inset* shows a dipole-type bead, and the red/green arrows mark displacement directions with respect to $\hat{N}_0$. (*B*) Trap stiffness $\alpha_{\parallel}$, $\alpha_{\perp}$ vs. power. Color scale of n_{eff} is the same as in Fig. 2.

the far-field director $\hat{N}_0$ than perpendicular to it (Fig. 4 *A* and *B*), consistent with the theory (13, 27) and recent experiments (28). We determine diffusion coefficients $D_{\parallel/\perp} = \Delta_{\parallel/\perp}^2/2\tau$ and find the ratio $D_{\parallel}/D_{\perp} = 1.9$ for AMLC-0010. However, the trapping force $F_t(W)$ quickly becomes much larger than F_{VD} when power is increased. Consequently, the particle displacements become small fractions of their values during free diffusion and $\Delta_{\parallel}$ becomes smaller than $\Delta_{\perp}$ (Fig. 4*B*). The maximum of the angular probability of the particle's displacements changes from directions along $\hat{N}_0$ to that perpendicular to $\hat{N}_0$ (Fig. 4*A*).

We reconstruct the optical trapping potential vs. distance between a colloid and the beam center for directions along and perpendicular to $\hat{N}_0$ (Fig. 5*A*). Fitting these results with a harmonic potential, we obtain the trap stiffness $\alpha_{\parallel/\perp}$ for different powers W (Fig. 5*B*). The dependencies $\alpha_{\parallel}(W)$ and $\alpha_{\perp}(W)$ are linear functions up to the power ($\approx$40 mW) at which we start to observe in PM the laser-induced director realignment around the bead (1). The stiffness is larger along $\hat{N}_0$, $\alpha_{\parallel} > \alpha_{\perp}$. The anisotropic properties of viscous and trapping forces for a dipolar colloid in Fig. 5*A* are different ($F_{VD\parallel} < F_{VD\perp}$ but $F_{t\parallel} > F_{t\perp}$), explaining why the particle displacements are easier along $\hat{N}_0$ than perpendicular to $\hat{N}_0$ only at small W (Fig. 4) and become more difficult at high W. When F_{VD} becomes negligible as compared with F_t at high W, probability vs. angle θ mimics the RIC (Fig. 4*A*). Anisotropic stiffness and particle dynamics are also observed for other types of colloids shown in Fig. 1 and will be reported elsewhere.

Trapping Forces. To further explore properties of trapping forces, we choose two types of samples with quadrupolar MR beads suspended (*i*) in 5CB with $n_o < n_p < n_e$ and (*ii*) in AMLC-0010 with $n_o < n_e < n_p$. We first trap a particle and then suddenly displace the beam to a distance $r > R$. The bead eventually follows the shift of the beam, but there is a lag of response at $r \geq R$ (Fig. 6).

We record the particle positions vs. time $r(t)$ and then calculate the trapping force that is balanced by the viscous drag: $F_t(r) = -\gamma(\theta)\partial r/\partial t$ (Fig. 7*A*). In our experiments, the Reynolds number
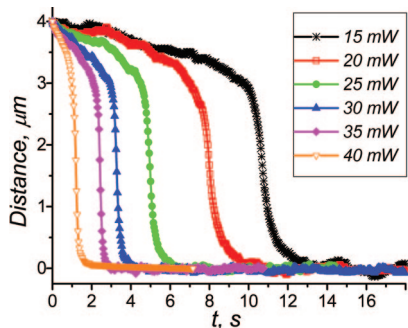

Fig. 6. Distance of the MR bead from the beam center vs. time as the beam is suddenly shifted by 4 μm along $\hat{N}_0$ in 5CB at different powers.
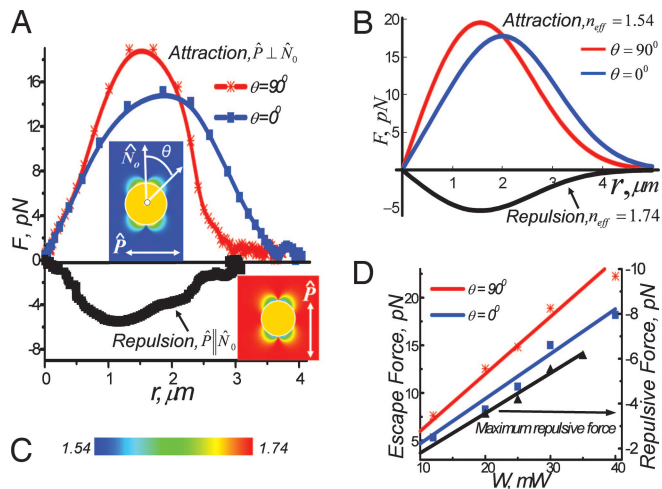

Fig. 7. Anisotropic trapping forces. (*A* and *B*) Optical forces acting on an MR bead of diameter 3 μm in 5CB obtained experimentally (*A*) and calculated by using Eq. 1 for effective sizes $l_{\parallel} = 4$ μm, $l_{\perp} = 3$ μm, and n_{eff} values marked on the figure (*B*). (*C*) Color scale of n_{eff}. (*D*) Trap escape force at $\hat{P} \perp \hat{N}_0$ for $\theta = 0°$, 90° and maximum repulsive force at $\hat{P} \parallel \hat{N}_0$ vs. power. The *Insets* in *A* show RICs at the two orthogonal polarizations.

(ratio of inertial and viscous forces) is much smaller than unity, which justifies the use of the Stokes law. At the experimental particle velocities <10 μm/s, the Ericksen number (ratio of viscous and elastic forces) is also smaller than unity, which allows us to neglect the nonlinear effects due to coupling between the director and velocity fields (13, 27). The later assumption is also justified by polarizing microscopy of textures around the moving beads, which do not show noticeable structure changes. We therefore use the effective anisotropic drag coefficients for different directions with respect to $\hat{N}_0$ obtained from the Brownian motion analysis.

The trapping force F_t dependencies on the bead–beam distance r qualitatively resemble those in isotropic fluids (29, 30) (Fig. 7*A*). $F_t(r)$ is a linear function at small r, has a maximum corresponding to the so-called escape force (19) at $r \sim R$, and decreases afterward, becoming negligible at distances $r > 2R$. Unlike in ordinary fluids, anisotropy of $F_t(r)$ is apparent (Fig. 7). Optical forces can be changed from attractive to repulsive (Fig. 7 *A* and *B*) by switching the linear polarization $\hat{P}$ to orthogonal, because the particle's index is in between n_o and n_e. The amplitude of repulsive force first increases with distance r, exhibits a maximum at typical $r \sim R$, and becomes negligible at $r > 1.5R$ (Fig. 7). The maxima of attractive and repulsive forces linearly increase with power, provided that it does not exceed the threshold value at which the beam starts to realign the director (Fig. 7*D*). The repulsive forces at $\hat{P} \parallel \hat{N}_0$ for MR bead in 5CB are weaker than the attractive forces at $\hat{P} \perp \hat{N}_0$, because $n_p \approx 1.68$ is closer to n_e than to n_o (Table 1) (i.e., the refractive index contrast is stronger for $\hat{P} \perp \hat{N}_0$).

The polarization effects on trapping forces are also present when $n_o < n_e < n_p$ (MR beads in AMLC-0010) (Fig. 8). Force F_t is larger for polarization perpendicular to $\hat{N}_0$ than for $\hat{P} \parallel \hat{N}_0$ (Fig. 8), due to a stronger refractive index contrast in the former case. Force F_t remains substantial up to larger distances when $\hat{P} \perp \hat{N}_0$, consistent with the respective RICs (Fig. 8 *Insets*). There is also some angular force variation, even though it is weaker than for the high-birefringence 5CB (Fig. 7). To further verify that the force anisotropy is caused by the symmetry of LC molecular alignment and RIC, we did testing experiments in an isotropic phase and also in a cholesteric LC with a strongly twisted director. We indeed observe that F_t in the beam's lateral plane becomes isotropic and polarization independent, which
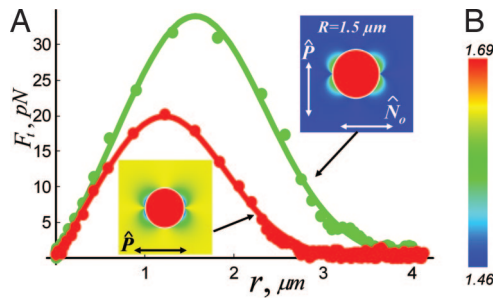
PHYSICS

Fig. 8. Polarization-controlled trapping forces. (*A*) Force F_t vs. distance r for polarizations $\hat{P} \perp \hat{N}_0$ and $\hat{P} \parallel \hat{N}_0$, as shown in the *Insets*. The solid curves are the best fits using Eq. **1** with $n_{eff} = 1.45$, $l_\parallel = 3.12$ μm for $\hat{P} \perp \hat{N}_0$ and $n_{eff} = 1.54$, $l_\parallel = 2.5$ μm for $\hat{P} \parallel \hat{N}_0$. (*B*) Color scale of n_{eff}.

shows that the studied anisotropic trapping properties are unique for anisotropic fluids.

Trapping in Biological Fluids. In addition to thermotropic LCs, we also studied trapping in biological anisotropic fluids: aqueous solutions of λ phage DNA with optical anisotropy $\Delta n = n_e - n_o < 0$ and FD virus with $\Delta n > 0$. In both cases, $|\Delta n| < 0.01$ is small and the average LC index $\bar{n}_{LC} = [(2n_o^2 + n_e^2)/3]^{1/2}$ is close to that of water $n_w = 1.33$. The anisotropy of trapping forces F_t in these systems is observed (~10%) when trapping silica beads with $n_p = 1.45$. However, optical trapping is strong but direction insensitive for MR particles with $n_p = 1.69$. Moreover, F_t in the latter case is essentially polarization independent. This result is expected because for MR beads $n_p = 1.69$ is much larger than n_e and n_o, and Δn is small. In addition, the particles in LCs of DNA and FD virus have weak tangential surface anchoring so that the bead distorts the director only in its close vicinity (Fig. 1*D*) and the trapping anisotropy effects are weak. Similar results are obtained for high-index MR beads in ZLI2806 of low Δn that we used to study elasticity-mediated forces (19).

Discussion and Conclusions

Our results demonstrate that trapping forces in anisotropic fluids are in general anisotropic, even for beads larger than the trapping beam wavelength λ_t. This result is in contrast to results in isotropic media, where particle dynamics in the linearly polarized traps can be anisotropic only for nanoparticles of radius $R < \lambda_t$; the anisotropy is averaged out if $R = \lambda_t$ or larger (31). Thus, the demonstrated direction-sensitive optical trapping of microparticles is a unique property of anisotropic media. Because of the RIC, the spherical beads exhibit trapping properties reminiscent of those of objects with an anisotropic shape, such as elongated cylinders (for colloids in Fig. 1*E*) and oblate discs (Fig. 1*G*). Their trapping can be controlled by multiple means, such as changing beam polarization, modifying the particles' surface treatment, using different LCs and chamber thicknesses, and applying external fields to change RIC. We now try to understand these properties in terms of a simple model.

We calculate the force acting on a bead near a focused beam. We take into account that refractive index $n_{eff}(\hat{P})$ varies from n_o to n_e, depending on polarization $\hat{P}$, and that a spherical bead with the RIC is essentially a colloid of anisotropic shape and some polarization-dependent effective sizes $l_\parallel$ and $l_\perp$ along and perpendicular to the far-field director $\hat{N}_0$, respectively. We account for gradient forces and adopt the assumption of Tlusty *et al.* (30) that the optical trap with field $\vec{E}(r, z)$ is formed by an axially symmetric three-dimensional Gaussian beam. The bead-trap interaction energy is $f(r) = (\varepsilon_0/2)[n_{eff}^2(\hat{P}) - n_p^2]\int_{V_c} \vec{E}(r, z)^2 dV$, where ε_0 is vacuum permittivity, beam axis is along $\hat{z}$, and integration is performed over the colloid's effective volume $V_e = l_\parallel l_\perp^2$. Taking the gradient of $f(r)$, we

find the force vs. distance from the trap center in the lateral plane for directions along and perpendicular to $\hat{N}_0$,

$$F_{t\parallel/\perp}(r) = \frac{2\omega^2 \alpha_{\parallel/\perp}}{l_{\parallel/\perp}} \exp\left[-\frac{r^2}{2\omega^2}\right] \sinh\left[\frac{rl_{\parallel/\perp}}{2\omega^2}\right], \quad \textbf{[1]}$$

and the trap stiffness

$$\alpha_{\parallel/\perp} = 2l_{\parallel/\perp}\xi[n_p^2/n_{eff}^2(\hat{P}) - 1]\frac{W}{c\omega^2}\,\text{erf}\left[\frac{l_{\parallel/\perp}}{2\sqrt{2}\omega}\right]$$

$$\text{erf}\left[\frac{l_\perp}{2\sqrt{2}\omega\xi}\right]\exp\left[\frac{-l_{\parallel/\perp}^2}{8\omega^2}\right], \quad \textbf{[2]}$$

where c is the speed of light, W is power, ω is an effective size of the beam's waist, and ξ is the ratio between the sizes of a focused beam along and perpendicular to $\hat{z}$. Eq. **1** explains the attraction of a particle to the trap for $n_p > n_{eff}(\hat{P})$ and repulsion when $n_p < n_{eff}(\hat{P})$ (Figs. 2, 7, and 8). At small distances r, one finds that $F_{t\parallel/\perp}(r) \approx \alpha_{\parallel/\perp}r$, as observed experimentally (Figs. 7 and 8). Calculated forces reproduce the experimental results such as force maximum at $r \sim R$ corresponding to the escape force (21) (Fig. 7 *A* and *B* and Fig. 8*A*). Eqs. **1** and **2** qualitatively describe direction sensitivity of forces (Fig. 7 *A* and *B*) and trap stiffness (Fig. 5), which are caused by different effective sizes $l_\parallel$ and $l_\perp$ of the LC colloids at angles $\theta = 0°$ and 90° to $\hat{N}_0$. Clearly, trapping forces in Fig. 7*A* remain strong up to larger distances along $\hat{N}_0$ than that perpendicular to $\hat{N}_0$, because the RIC is wider for $\theta = 0°$ ($l_\parallel > l_\perp$). We use Eq. **1** to fit experimental data in Fig. 8; the obtained fitting parameters $n_{eff}(\hat{P})$ and $l_\parallel$ agree with expected values. As compared with the bead diameter, the effective size of LC colloids is larger ($l_\parallel > 2R$) for $\hat{P} \perp \hat{N}_0$ and smaller ($l_\parallel < 2R$) for $\hat{P} \parallel \hat{N}_0$, due to a larger/smaller index in respective RICs as compared with $n_{eff}(\hat{P})$ far from the beads (Fig. 8 *Insets*).

Using Eq. **1**, one finds that the trapping force can be polarization controlled from its minimum $F_{t_{min}}$ at $\hat{P} \parallel \hat{N}_0$ to the maximum $F_{t_{max}}$ at $\hat{P} \perp \hat{N}_0$:

$$\frac{F_{t_{max}} - F_{t_{min}}}{F_{t_{max}}} = \frac{n_p^2(n_o + n_e)\Delta n}{n_e^2(n_p^2 - n_o^2)}. \quad \textbf{[3]}$$

This finding explains, for example, why optical trapping of high-index MR beads in LCs of DNA and FD virus with low birefringence is less polarization sensitive than in the case of silica beads. Moreover, according to Eqs. **1-3**, optical trapping can be strongly anisotropic and polarization controlled even in biological fluids with low Δn provided that the particle's index is between n_o and n_e. Quantitative agreement is good for LCs with low optical anisotropy Δn (Fig. 8) and somewhat worse in 5CB with high Δn (Fig. 7) (where some light depolarization/defocusing and director reorientation effects might take place). The presented model allows one to understand polarization-dependent anisotropic trapping in anisotropic fluids at laser powers that do not reorient $\hat{N}$ (20, 32). Further model improvement would require using the actual field distribution of the focused beam (31), calculating director structures for finite surface anchoring and anisotropic elasticity (3), as well as taking into account scattering forces (2), light defocusing/depolarization effects in birefringent media (21), and induced director distortions at high laser powers (20, 32).

Our results impinge on laser tweezers studies of anisotropic materials such as measurements of viscosity coefficients and interaction forces. It is important to either perform force/stiffness calibration for different directions with respect to $\hat{N}_0$ or to mitigate this experimental complexity by using circularly polarized optical traps or/and using low-birefringence LCs along with high-index particles $n_p \gg n_o$ and n_e as in our previous study

Smalyukh *et al.*

(19, 21). This behavior is in contrast to that in isotropic fluids, where calibration for only one direction in the lateral plane is sufficient (2). Moreover, Fig. 5*B* demonstrates that quantitative studies can be performed only for relatively low power. The measurements are easier in materials with low Δn for which the director reorientation is weaker and starts at a higher threshold power (32); thus, stronger trapping forces can be generated without reorienting the director (19, 21).

Polarization sensitivity of trapping forces in anisotropic fluids is of both fundamental and applied interest. For example, it can be used for constructing model thermodynamic systems with anisotropic potential wells. According to Eq. **1**, high-birefringence fluids allow optical forces to be controlled by polarization within a broader range and are useful for such applications. The polarization-controlled motion of particles into/away from a stationary trap may find applications in light-controlled microfluidics devices, nano- and micropumps, optomechanic sensors and transducers, etc. The effect could potentially be used for dynamic rearranging of periodic bead arrays and for optical tuning or creating defects in photonic crystals infiltrated by LCs. Moreover, switching between different RICs can provide a further control of particle motions by an external electric field.

To conclude, we have demonstrated direction-sensitive and polarization-controlled optical trapping of particles in anisotropic fluids and described these properties by using a simple model. Particle dynamics and trapping forces mimic the director structure and the RIC around an immersed bead. The findings are applicable to a broad range of anisotropic fluids, including those of biological significance, and impinge on their quantitative study using laser tweezers.

Materials and Techniques

Materials and Sample Preparation. LC chambers were assembled from plates coated with polyimide PI2555 (HD MicroSystems, Parlin, NJ) alignment layers buffed to set a uniform far-field director $\hat{N}_0$ (21). The glass plates had a refractive index of 1.52 and thickness of 0.15 mm, to minimize spherical aberrations when using oil-immersion objectives. The sample thickness $h = 5$–50 μm was set by using strips of Mylar films placed along chamber edges. After the chamber was sealed by using a UV-curable glue, h was measured by using the interference method. The samples were prepared by using a nematic 5CB or a mixture AMLC-0010 (33) with ordinary n_o, extraordinary n_e, and average $\bar{n}_{LC}$ refractive indices provided in Table 1. We used melamine resin particles (Aldrich, Milwaukee, WI) of refractive index $n_p \approx 1.68$ and radius $R = 1.5$ μm and glass (soda lime) particles with $n_p \approx 1.51$ and $R = 1$ μm (Duke Scientific, Palo Alto, CA). Particles were treated either with lecithin to induce perpendicular orientation of LC molecules to their surface or with polyisoprene for the parallel orientation (19). LC and well

separated particles were introduced into the chamber by capillary forces. During the sample loading, materials were heated to temperatures above the nematic–isotropic transition to avoid flow effects on the LC alignment, and then they were slowly cooled down to room temperatures. Studied materials are transparent at the trapping wavelength $\lambda_t = 1,064$ nm and in the visible spectral range of microscopy studies. No induced sample heating of more than 1°C was observed.

We used anisotropic fluids of FD virus (34) and DNA (10). The LC phase of λ DNA (contour length = 16.3 μm, persistence length ≈ 50 μm; New England Biolabs, Ipswich, MA) was prepared by drying a droplet of aqueous DNA at initial 5 mg/ml until the LC formed (10). Anisotropic fluids of FD virus rods (length 0.88 μm, diameter 6.6 nm, at 56 mg/ml in water) were prepared according to standard protocols (34). These materials have optical anisotropy $\Delta n = n_e - n_o$ two orders of magnitude smaller than in thermotropic LCs, $|\Delta n| < 0.01$; $\Delta n < 0$ for the DNA LC and $\Delta n > 0$ for the FD virus LC. Using materials of different origin, various values of Δn, and different particles with n_p larger, smaller, or in between the indices n_e and n_o allows us to generalize our conclusions to a broad spectrum of anisotropic fluids.

Trapping and Imaging Techniques. We used a dual-beam trapping system consisting of an LM-2 optical manipulator (Solar-TII, Minsk, Belarus), a Compass 1064-2000 TEM$_{00}$ continuous-wave Nd:YAG laser (Coherent, Santa Clara, CA), and a TE-200 microscope (Nikon Instruments, Melville, NY). The laser power was varied within $W = 0$–60 mW. An optical trap was formed by using a $\times 100$ objective (numerical aperture = 1.3) with $\sim 40\%$ transmission at $\lambda_t = 1,064$ nm. The focused beam was steered in the horizontal plane by a computer-controlled galvano-mirror pair and visualized by a colocalized beam of a HeNe laser ($\lambda = 633$ nm). The vertical z coordinate of the trap was controlled by a piezostage with 0.1-μm accuracy. Simultaneously with the optical trapping, we conducted polarizing microscopy and bright-field optical microscopy observations using a Cascade 650 charge-coupled device (CCD) camera (Roper Scientific, Trenton, NJ) and a MicroPublisher 3.3 real-time viewing camera (QImaging, Burnaby, BC, Canada). The particle motion and texture changes were monitored at rates up to 200 frames per second. The position of the particle's center of gravity was determined by a computer analysis of microscopy images and particle tracking routines (19) with ± 3-nm accuracy.

1. de Gennes P-G, Prost J (1993) *The Physics of Liquid Crystals* (Clarendon, Oxford), 2nd Ed.
2. Prasad PN (2003) *Introduction to Biophotonics* (Wiley, New York).
3. Chaikin PM, Lubensky TC (1995) *Principles of Condensed Matter Physics* (Cambridge Univ Press, Cambridge, UK).
4. Collings PJ, Hird M (2001) *Introduction to Liquid Crystals: Chemistry and Physics* (Taylor & Francis, London).
5. Hulmes DJ (2002) *J Struct Biol* 137:2–10.
6. Blanc NS, Senn A, Leforestier A, Livolant F, Dubochet J (2001) *J Struct Biol* 134:76–81.
7. Livolant F (1991) *Physica A* 176:117–137.
8. Nazzal S, Smalyukh II, Lavrentovich OD, Khan MA (2002) *Int J Pharm* 235:247–265.
9. Zribi O, Kyung H, Golestanian R, Liverpool T, Wong GCL (2005) *Europhys Lett* 70:541–547.
10. Smalyukh II, Zribi OV, Butler JC, Lavrentovich OD, Wong GCL (2006) *Phys Rev Lett* 96:177801.
11. Vollrath F, Knight DP (2001) *Nature* 410:541–548.
12. Poulin P, Stark H, Lubensky TC, Weitz DA (1997) *Science* 275:1770–1773.
13. Stark H (2001) *Phys Rep* 351:387–474.
14. Coleman DA, Fernsler J, Chattham N, Nakata M, Takanishi Y, Körblova E, Link DR, Shao, R-F, Jang WG, Maclennan JE, *et al.* (2003) *Science* 301:1204–1211.
15. Fishkind DJ, Wang Y (1993) *J Cell Biol* 123:837–848.
16. Katoh K, Hammar K, Smith PJ, Oldenbourg R (1999) *Mol Biol Cell* 10:197–210.
17. Yada M, Yamamoto J, Yokoyama H (2004) *Phys Rev Lett* 92:185501.
18. Ivashita Y, Tanaka H (2003) *Phys Rev Lett* 90:045501.
19. Smalyukh II, Lavrentovich OD, Kuzmin AN, Kachynskii AV, Prasad PN (2005) *Phys Rev Lett* 95:157801.
20. Škarabot M, Ravnik M, Babič D, Osterman N, Poberaj I, Žumer S, Muševič I, Nych A, Ognysta U, Nazarenko V (2006) *Phys Rev E* 73:021705.
21. Smalyukh II, Kuzmin AN, Kachynskii AV, Prasad PN, Lavrentovich OD (2005) *Appl Phys Lett* 86:021913.
22. Pattanaporkratana A, Park CS, Maclennan JE, Clark NA (2004) *Ferroelectrics* 310:131–136.
23. Prasad PN (2004) *Nanophotonics* (Wiley, New York).
24. Loudet JC, Mondain-Monval O, Poulin P (2002) *EuroPhys J E* 7:205–208.
25. Lubensky TC, Pettey D, Currier N, Stark H (1998) *Phys Rev E* 57:610–625.
26. Ruhwandl RW, Terentjev EM (1997) *Phys Rev E* 55:2958–2961.
27. Stark H, Ventzki D (2002) *Europhys Lett* 57:60–66.
28. Loudet J, Hanusse P, Poulin P (2004) *Science* 306:1525.
29. Simmons RM, Finer JT, Chu S, Spudich JA (1996) *Biophys J* 70:1813–1822.
30. Tlusty T, Meller A, Bar-Ziv R (1998) *Phys Rev Lett* 81:1738–1741.
31. Rohrbach A (2005) *Phys Rev Lett* 95:168102.
32. Durbin SD, Arakelian SM, Shen YR (1981) *Phys Rev Lett* 47:1411–1414.
33. Smalyukh II, Senyuk BI, Palffy-Muhoray P, Lavrentovich OD, Huang H, Gartland EC, Bodnar V, Kosa T, Taheri B (2005) *Phys. Rev. E* 72:061707.
34. Purdy KR, Dogic Z, Fraden S, Ruhm A, Lurio L, Mochrie SGJ (2003) *Phys Rev E* 67:031708.

PHYSICS

Smalyukh *et al.*

www.manaraa.com